Contents lists available at ScienceDirect

Journal of Luminescence

journal homepage: www.elsevier.com

Excited state luminescence signals from a random distribution of defects: A new Monte Carlo simulation approach for feldspar

Vasilis Pagonis[a,*], Johannes Friedrich[b], Michael Discher[c], Anna Müller-Kirschbaum[b], Veronika Schlosser[b], Sebastian Kreutzer[d], Reuven Chen[e], Christoph Schmidt[b]

[a] Physics Department, McDaniel College, Westminster, MD 21157, USA
[b] Chair of Geomorphology, University of Bayreuth, 95440 Bayreuth, Germany
[c] Department of Geography and Geology, University of Salzburg, Hellbrunner Str. 34, 5020 Salzburg, Austria
[d] IRAMAT-CRP2A, UMR 5060 CNRS - Université Bordeaux Montaigne, Maison de l'Archéologie, Esplande des Antilles, 33607 Pessac cedex, France
[e] Raymond and Beverly Sackler School of Physics and Astronomy, Tel Aviv University, Tel Aviv 69978, Israel

ARTICLE INFO

Keywords:
Monte Carlo model
Feldspar model
Excited state luminescence in feldspars

ABSTRACT

This paper presents Monte Carlo simulations of tunneling recombination in random distributions of defects. Simulations are carried out for four common luminescence phenomena in solids exhibiting tunneling recombination, namely continuous wave infrared stimulated luminescence (CW-IRSL), thermoluminescence (TL), isothermal thermoluminescence (iso-TL) and linearly modulated infrared stimulated luminescence (LM-IRSL). Previous modeling work has shown that these phenomena can be described by the same partial differential equation, which must be integrated numerically over two variables, the elapsed time and the donor-acceptor distance. We here present a simple and fast Monte Carlo approach which can be applied to these four phenomena, and which reproduces the solution of the partial differential equation, without the need for numerical integrations. We show that the method is also applicable to cases of truncated distributions of nearest neighbor distances, which characterize samples that underwent multiple optical or thermal pretreatments. The accuracy and precision of the Monte Carlo method are tested by comparing with experimental data from several feldspar samples.

1. Introduction

Recent experimental and modeling work has contributed to a better understanding of the nature and origin of thermally and optically luminescence processes in feldspars (see for example the recent review paper by Pagonis et al. [1]). The model developed by Jain et al. [2] has provided a framework for the description of tunneling phenomena in dosimetric materials, based on a random distribution of donor-acceptor pairs. Kitis and Pagonis [3] quantified the semi-analytical model of Jain et al. [2], by deriving analytical expressions for different experimental stimulation modes. These analytical equations were used to describe luminescence signals from a variety of feldspars and apatites, namely continuous wave infrared stimulated luminescence (CW-IRSL), thermoluminescence (TL), isothermal luminescence (ITL) and linearly modulated infrared stimulated luminescence (LM-IRSL) ([4–8]). Jain et al. [9] extended their localized transition model to include Arrhenius analysis, and to develop approximate equations based on truncated nearest neighbor distributions. Their extended model successfully described the experimentally observed thermal and optical kinetic behavior of IRSL signals from preheated feldspar samples [9].

In recent literature, Monte Carlo (MC) simulations were used to describe luminescence signals in dosimetric materials. In general, MC approaches can be implemented to run three types of models: (I) models based on delocalized transition between the two energy bands ([10–14]), (II) models based on localized transitions involving different energy levels within the traps/centers ([15–18]) and (III) semi-localized models which basically combine recombination routes including both delocalized and localized states [19]. The paper by Horowitz et al. [20] and the book by Chen and Pagonis [21] provide a good overview of these types of luminescent models.

In addition to the above modeling studies, MC methods have been used to describe the behavior of luminescence signals from nanodosimetric materials, in which variable-sized clusters of traps and recombi-

* Corresponding author.
Email address: vpagonis@mcdaniel.edu (V. Pagonis)

https://doi.org/10.1016/j.jlumin.2018.11.024
Received 20 September 2018; Received in revised form 9 November 2018; Accepted 13 November 2018
Available online xxx

nation sites are considered as separate, non-interacting systems ([22,23]). Since there is no analytical solution to describe these phenomena, MC methods must be used to simulate their behavior ([15,17]).

The specific goals of this paper are:

- To develop a simple and efficient MC method that can be applied to CW-IRSL, LM-IRSL, isothermal luminescence and TL phenomena, without the need for numerical integrations.
- To test the accuracy and precision of this MC method, and to compare it with experimental data.
- To apply this method to truncated distributions of nearest neighbor distances, which characterize samples that underwent optical or thermal pre-treatments.

2. Experimental and samples

Unless otherwise specified, the luminescence measurements in this paper were carried out using a Risø TL/OSL reader (model TL/OSL-DA-15), equipped with a $^{90}Sr/^{90}Y$ beta particle source, delivering a nominal dose rate of ca. 0.075 Gy/s. A 9635QB photomultiplier tube (PMT) was used with a 7.5 mm Hoya U-340 filter (~340 nm, FWHM ~80 nm). For the prompt isothermal measurements reported in this paper, a combination of Pilkington HA-3 heat absorbing and Corning 7–59 (320–440 nm) blue filter were used in front of the PMT. The IRSL stimulation wavelength is 875 (±40) nm and the maximum power density ~135 mW/cm^2. All measurements were performed in a nitrogen atmosphere with a low constant heating rate of 1–2 K/s, in order to avoid significant temperature lag. The samples were heated up to the maximum temperature of 500 °C.

Several of the measurements were carried out using a microcline sample (laboratory code KST4), studied previously in Polymeris et al. ([24,25]) and Pagonis et al. [26]. Prompt isothermal decay measurements were carried out using a Durango apatite sample known for exhibiting strong anomalous fading [5]. The single piece natural apatite crystal with dimensions of 8 × 4 × 3 mm was crushed gently with an agate mortar, to obtain the grain size fraction 80–140 μm which were annealed at 900 °C in air for 1 h in order to empty all traps, followed by rapid cooling to room temperature. 5 mg aliquots were attached to stainless steel disks.

The LM-IRSL feldspar data analyzed in this paper were previously published by Bulur and Göksu [27]. These authors studied the fine powders of K and Na feldspar standards (samples NBS-70a and NBS-99a) by using IR LEDs with a maximum power density setting of 40 mW/cm^2. The LM-IRSL data was obtained after irradiating the feldspars with a dose of 2.5 Gy and preheating the samples at 200 °C for 5 min.

3. Brief review of the model by Jain et al. [2]

The model of Jain et al. [2] bases on localized electronic recombination within a system of random distribution of pairs of trapped electrons and recombination centers, and the transitions are shown schematically in Fig. 1. Recombination is assumed to take place via tunneling from the excited state of the trapped electron and takes place only to the nearest neighbor centers.

In the exact form of the model presented by Jain et al. [2], the differential equations are:

$$\frac{\partial n_g\left(r',t\right)}{\partial t} = -An_g\left(r',t\right) + Bn_e\left(r',t\right), \tag{1}$$

$$\frac{\partial n_e\left(r',t\right)}{\partial t} = An_g\left(r',t\right) - Bn_e\left(r',t\right) - \frac{n_e\left(r',t\right)}{\tau\left(r'\right)}, \tag{2}$$

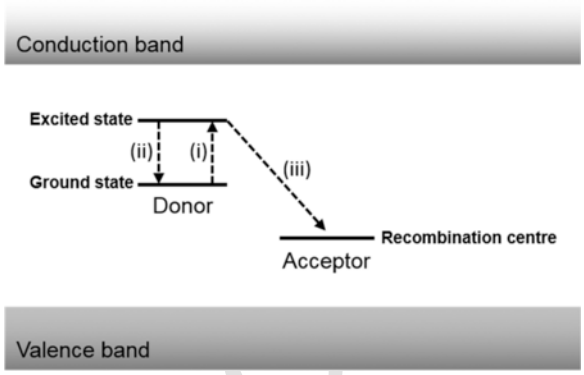

Fig. 1. Simplified energy-band diagram showing the electronic transitions discussed in the text: transition (i) denotes the thermal or optical excitation from the ground state of the trapped electron to the excited state, and transition (ii) is de-excitation back into the ground state. Transition (iii) is direct tunneling from the excited state of the trapped electron to the recombination center.

$$L\left(t\right) \propto \int_0^\infty \frac{n_e\left(r',t\right)}{\tau\left(r'\right)} dr', \tag{3}$$

$$\tau\left(r'\right) = s_{tun}^{-1} \exp\left(\frac{r'}{\left(\rho'\right)^{1/3}}\right). \tag{4}$$

Here one defines the dimensionless distance parameter $r' = (4\pi\rho/3)^{1/3}r$, where ρ (m^{-3}) represents the actual density of recombination centers in the material. Similarly, one introduces the dimensionless density of recombination centers parameter by $\rho' = (4\pi\rho/3)\alpha^{-3}$, where α(m^{-1}) is the potential barrier penetration constant (Jain et al. [2]). $n_g(r',t)$ and $n_e(r',t)$ (both m^{-3}) are the instantaneous concentrations of electrons in the ground state and in the excited state correspondingly, and these are functions of time t (s) and of the distance parameter r'. In the above equations s_{tun}(s^{-1}) is the frequency factor characterizing the tunneling process taking place from the excited state of the system, A (s^{-1}) is the excitation rate from the ground to the excited state (transition i, Fig. 1), and B (s^{-1}) is the rate of de-excitation from the excited state back to the ground state (transition ii, Fig. 1). From a physical point of view, there is no relationship between the three different frequency factors A, B and s_{tun}. The tunneling lifetime $\tau(r')$ (s) depends on the distance r' and $L(t)$ is the instantaneous photon emission rate resulting from tunneling recombination via the excited state (transition iii, Fig. 1).

The system of differential Eqs. (1)–(4) can be solved numerically for known numerical values of the parameters. As mentioned in the Introduction section, Kitis and Pagonis [3] derived approximate analytical solutions for this system of equations, and for different experimental stimulation modes. Besides, Pagonis et al. [30] examined the exact version of the model and developed analytical equations for the concentration of carriers during measurement of luminescence signals, as a function of the dimensionless distance parameter r' and of the stimulation time t.

Pagonis et al. [28] showed that using the quasi-equilibrium condition $\partial n_e(r',t)/\partial t \sim 0$, and assuming that $n_e << n_g$, the system of Eqs. (1)–(4) can be replaced with the following single differential equation ([30], their Eq. (9)):

$$\frac{\partial n_g\left(r',t\right)}{\partial t} = -\frac{As_{tun}}{B\exp\left[\left(\rho'\right)^{-1/3}r'\right]} n_g\left(r',t\right), \tag{5}$$

with the symbols used here defined as previously.

As discussed in [28], Eq. (5) can be integrated formally for a constant distance r', to yield the total concentration of electrons in the ground state at time t and for a fixed distance parameter r':

$$n_g(r',t) = n_g(r',0)\exp\left[-\frac{s_{tun}}{B\exp\left[(\rho')^{-1/3}r'\right]}\int_0^t A dt'\right], \quad (6)$$

where $n(r',0)$ represents the initial concentration of electrons in the ground state at time $t = 0$ corresponding to a distance r'. For a freshly irradiated sample, this initial distribution of electrons in the ground state at time $t = 0$ is given by the peak-shaped nearest-neighbor distribution function:

$$n_g(r',0) = 3n_0(r')^2\exp\left[-(r')^3\right], \quad (7)$$

where n_o is the total concentration of electrons in the ground state at time $t = 0$. By combining Eqs. (6) and (7):

$$n_g(r',t) = 3n_0(r')^2\exp\left[-(r')^3\right]\exp\left[-\frac{s_{tun}}{B\exp\left[(\rho')^{-1/3}r'\right]}\int_0^t A dt'\right]. \quad (8)$$

Eq. (8) describes the evolution of the distribution of electrons in the ground state as a function of the time t elapsed since the beginning of the optical or thermal stimulation. The integral $\int_0^t A dt'$ must be evaluated numerically or analytically for the different excitation modes. By integrating Eq. (8) over the distance variable r' and by combining with Eq. (4), one finds the total remaining number of electrons $n(t)$ in the ground state at time t:

$$n(t) = \int_0^\infty n_g(r',t)\ dr' = \int_0^\infty 3n_0(r')^2\exp\left[-(r')^3\right]\exp\left[-\frac{s_{tun}}{B\exp\left[(\rho')^{-1/3}r'\right]}\int_0^t A dt'\right]\ dr'. \quad (9)$$

In the rest of this paper $n(t)$ will be used to denote the total number of remaining trapped electrons in the ground state. The time-dependent luminescence intensity $L(t)$ is evaluated numerically from the equation:

$$L(t) = -\int_0^\infty \frac{\partial n_g(r',t)}{\partial t} dr'. \quad (10)$$

Eqs. (9) and (10) allow a numerical calculation of $n(t)$ and $L(t)$, by integrating numerically over the possible range of the dimensionless variable $r' = 0$ to $r' = \infty$. The physical meaning of Eq. (10) is that the TL signal can be represented by the summation (integral) of the terms $\frac{\partial n_g(r',t)}{\partial t}$, over all possible values of the dimensionless radius parameter r'.

The value of the parameter A depends on the stimulation mode used in the experiments. In the case of CW-IRSL experiments, the parameter A represents the constant rate of infrared excitation A_{IR}. In an isothermal decay experiment, the temperature T_{ISOTH} of the sample is kept constant and the parameter A is replaced by the constant rate of thermal excitation $A_{ISOTH} = s_{th}\exp(-E/k_BT_{ISOTH})$, where E (eV) is the thermal activation energy and s_{th} (s^{-1}) is the pre-exponential factor for the thermal excitation process, which is proportional to the lattice vibration frequency (McKeever, [29], page 48) and where k_B is the Boltzmann constant (eV K^{-1}). In a TL experiment, the sample is heated with a linear heating rate β (K s^{-1}), from a starting temperature T_o up to a high temperature around 500 °C, so that the temperature varies as $T(t) = T_o + \beta t$. In this case the parameter A is replaced by the time-dependent probability of thermal excitation $A_{TL} = s_{th}\exp[-E/k_BT(t)]$. During LM-IRSL experiments, the probability of optical excitation A is varied linearly with time in the form $A = (bt)/T_{total}$, where T_{total} (s) is the total excitation period and b is an experimental constant.

Although standard numerical integration methods can be used to evaluate the integrals in Eqs. (9)–(10), this paper presents an alternative method based on MC techniques.

The MC method presented here provides an alternative method of evaluating both $n(t)$ and $L(t)$ simultaneously, without carrying out the numerical integrations in Eqs. (9) and (10). The advantages of using a MC method are:

(a) The method is fast, efficient and avoids numerical integration,
(b) it produces accurate results even in cases of low stimulation probability, in which it is known that the analytical equations of Kitis and Pagonis [3] are less accurate,
(c) it can be used for both freshly irradiated samples and for irradiated samples which underwent thermal or optical pre-treatments, by making a very small modification in the limits of integration.
(d) The method can also be used to describe clustering effects in nanodosimetric materials, by considering systems of traps and centers consisting of a small number of particles.

4. The Monte Carlo method

The MC method evaluates the total concentration of remaining electrons $n(t)$ and the luminescence intensity $L(t)$ simultaneously, based on the differential Eq. (5). In the MC simulations, Eq. (5) becomes a *difference* equation for the *discrete* variable n, in the general form:

$$\Delta n(r',t) = -\frac{As_{tun}}{B\exp\left[(\rho')^{-1/3}r'\right]} n(r',t)\,\Delta t, \quad (11)$$

where Δt is an appropriate time interval, e.g. $\Delta t = 1\ s$.

From a practical point of view, the integration indicated in Eqs. (9) and (10) does not need to extend to infinity, since the peak shaped function $3(r')^2\exp[-(r')^3]$ becomes practically zero for r' values larger than 2. Using this approximation, Eqs. (9) and (10) become finite sums:

$$n(t) = \sum_{r'=0}^{2} n(r',t)\ \Delta r', \quad (12)$$

$$L(t) = -\sum_{r'=0}^{2} \frac{\Delta n(r',t)}{\Delta t}\ \Delta r', \quad (13)$$

where $\Delta r'$ is an appropriate distance interval, e.g. $\Delta r' = 0.02$. The effect of using different values of Δt and $\Delta r'$ was tested by repeating the simulations using shorter intervals, and the simulation results stayed unaffected by changing the value of Δt and $\Delta r'$. The general Eqs. (11), (12) and (13) are the basis of the "brute force" MC method found in standard textbooks of simulations in Statistical Physics [14], and a simpler form of the method was also discussed in the paper by Pagonis et al. [13]. Software implementation proceeds as follows: the overall evolution of the system will be followed for *both* the time variable t, and for each value of the dimensionless distance r', by using two iterative loops. The inner loop is executed using a time variable t, and for a constant value of the distance parameter r'. The outer loop repeats the inside loop for all possible discrete values of the parameter $r' = r' + \Delta r'$. At time $t = 0$ there are n_o filled traps, and the distribution of nearest neighbors is given by the peak shaped function $n(r',0) = n_o3(r')^2\exp[-(r')^3]$. The rate P for an electron to recombine radiatively within the time interval Δt and for certain distance r' is given by the function $As_{tun}/\{B\exp[(\rho')^{-1/3}r']\}$ in the right hand side of Eq. (5). By following the same method as in Pagonis et al. ([13]), one chooses a suitable value of Δt so that $P\Delta t << 1$, and a random number r is generated, which is uniformly distributed in the unit interval $0 \le r < 1$. If $r \le P$ the electron recombines radiatively, otherwise it does not; all non-recombined remaining electrons in the system are tested in this manner during each time interval Δt, and several recombination events could take place during each time interval Δt. At the end of each time interval Δt, the program stores the values of $n(r',t)$, and $\Delta n(r',t)/\Delta t$.

This process is now repeated for the next value of the distance $r' = r' + \Delta r'$ in the outer software loop. Finally, the contributions from

all distances r' are added according to Eqs. (12) and (13), resulting in the simultaneous evaluation of the discrete-value functions $n(t)$ and $L(t)$. Both iterative loops are executed until there are no particles left in the system.

It is noted that the density of recombination centers in this type of model is considered to be a constant, and does not need to be updated during the Monte Carlo simulation. This is because one of the fundamental assumptions of the model is that the concentration of recombination centers far exceeds the concentration of electrons in the material under consideration.

The MC simulations reach a precision of 1% rather quickly, by repeating 10 cycles of 200 electrons each. The accuracy of the MC method is ascertained by comparing with the results from the exact model by Jain et al. [2], and is discussed in the next section.

The simulations in this paper were carried out using the commercial software package *Mathematica*. Typical running times for $N = 200$ electrons in the system are ~1–2 min, and the simulations use the random number generator embedded in *Mathematica*. No special packages or libraries are required for the straightforward simulations presented in this paper.

The above Eqs. (9)–(10) are strictly applicable *for freshly irradiated samples*. However, they can also be used for irradiated samples which were exposed to optical and thermal pre-treatments. Examples of such combined treatments are an IR bleaching followed by TL measurement, an IR treatment followed by isothermal decay, a partial heating followed by TL measurement etc. For such pre-treated samples, one can approximate the nearest neighbor distribution with a *truncated* distribution function, which extends from a minimum critical radius r'_c up to infinity ([2,9,25]). This critical radius can be treated as an adjustable modeling parameter when fitting experimental data. For such truncated distributions, Eqs. (9) and (10) will become:

$$n(t) = \int_{r'_c}^{\infty} 3n_0 (r')^2 \exp\left[-(r')^3\right] \exp\left[-\frac{1}{B\tau(r')}\int_0^t A dt'\right] dr', \quad (14)$$

$$L(t) = \int_{r'_c}^{\infty} \frac{A}{B\tau(r')} n(r',0) \exp\left[-\frac{1}{B\tau(r')}\int_0^t A dt'\right] dr'. \quad (15)$$

5. Results of the Monte Carlo simulations - comparison with the numerical solutions of the differential equations

Fig. 2 shows a MC simulation of an isothermal experiment for the Durango apatite sample, in which the temperature is raised to 220 °C and kept constant for 1000 s (Sfampa et al. [5]). The parameters in the MC simulation are $\rho' = 0.007$, $A_{ISOTH} = 0.20\ s^{-1}$. The gray area in Fig. 2a indicates the overall results from 10 MC simulations of 200 electrons each, and the dashed line indicates the average of these 10 runs. Fig. 2b compares the experimental data (open circles), with the MC simulation (dashed line) with the exact solution obtained by the numerical integration of Eq. (3) (solid line). The two simulation results (solid and dashed lines) in Fig. 2b are indistinguishable from each other. The fitting residuals shown at the bottom of Fig. 2b indicate good agreement of the order of 3% or better, between the experimental data, the numerical solution, and the MC results. The fitting residuals are defined here as the percent ratio (experimental-MC results)/(MC results).

Fig. 3a shows typical CW-IRSL data measured with microcline sample KST4, with a reduced IR-stimulating power of 10% of the maximum IR-intensity. The CW-IRSL from this sample were previously analyzed in Pagonis et al. [26], by using the analytical equations by Kitis and Pagonis [3]. The solid line shows the result of the MC simulation with the following parameters: ?′ = 0.003, $A_{IRSL} = 0.12\ s^{-1}$ and is practically indistinguishable from the numerical integration results of the full model ([2]). The experiment was also repeated with reduced

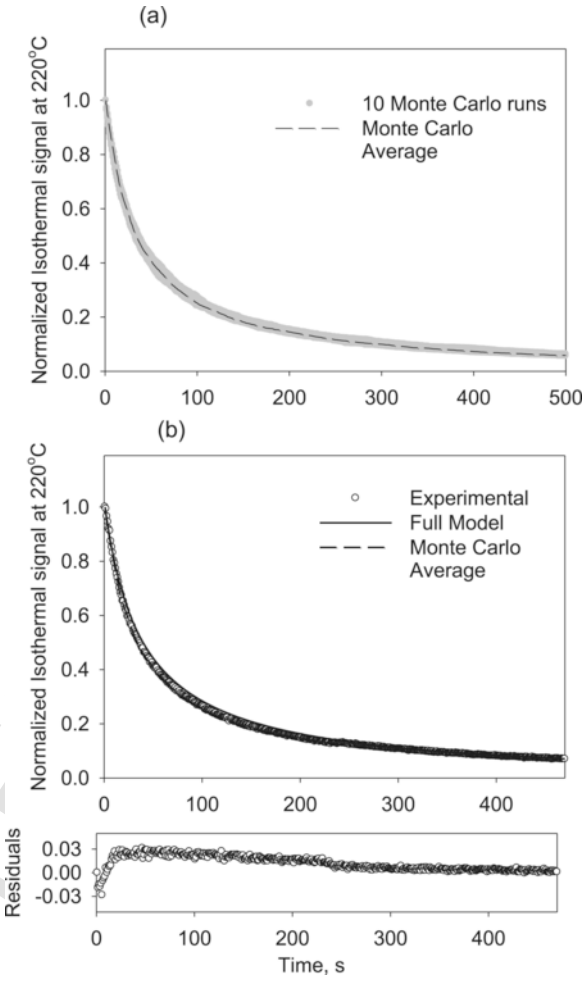

Fig. 2. (a) MC simulation of an isothermal experiment for irradiated Durango apatite. The temperature is raised to 220 °C and kept constant for 500 s (Sfampa et al., [5]). The parameters in the MC simulation are $\rho' = 0.007$, $A_{ISOTH} = 0.20\ s^{-1}$. The gray area in (a) indicates the overall results from 10 MC simulations of 200 electrons each, and the dashed line indicates the average of these 10 runs. (b) The experimental data (open circles) are compared with the MC simulation (dashed line), and with the exact solution obtained by the numerical integration of Eq. (3) (solid line). The fitting residuals shown are of the order of 3% or better.

powers of 20%, 30%, 40% of the maximum IR-intensity, with two of the fitted curves measured at powers 10% and 40% shown in Fig. 3b. The inset of Fig. 3b shows the linear relationship between the fitting parameter A_{IRSL} and the percent power used in the experiments.

As discussed above, the MC method can also simulate multiple-level experiments, in which samples are subjected to a combination of optical and thermal treatments. In these samples, one can use *truncated* distribution functions which extend from a minimum critical radius r'_c up to infinity. In order to test this method of fitting experimental TL glow curves, we have carried out a series of measurements shown in Fig. 4 and 5, in which a feldspar sample is irradiated and subsequently preheated for variable preheat times and at variable preheat temperatures. These experiments were carried out on a single aliquot of the microcline sample KST4 that was described in the experimental section. The sample in these measurements was given a test dose of 40 Gy and a preheat from room temperature up to a temperature of 300 °C, in order to remove the TL signal due to shallow traps.

In the experiment shown in Fig. 4, the irradiated sample was preheated to T_{PH}= 300 °C and subsequently this preheat temperature was held fixed for a variable preheat time .. s. In this *variable preheat time experiment*, it is assumed that these preheated samples can be described using a *truncated* distribution function, which extends from a minimum

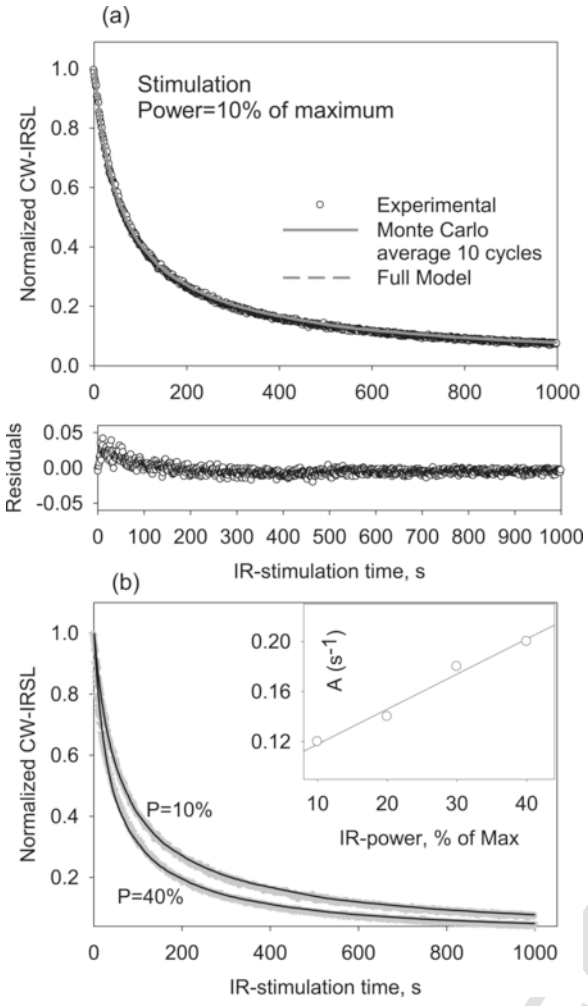

Fig. 3. (a) CW-IRSL data measured with sample KST4, with a reduced IR-stimulating power of 10% of the maximum IR-intensity. The solid line shows the result of the MC simulation with the parameters given in the text. (b) The experiment was repeated with reduced power densities of 20%, 30%, 40% of the maximum IR-power density, with two of the fitted curves measured at 10% and 40% shown here. The inset shows the linear relationship between the fitting parameter A_{IRSL} and the percent power used in the experiments.

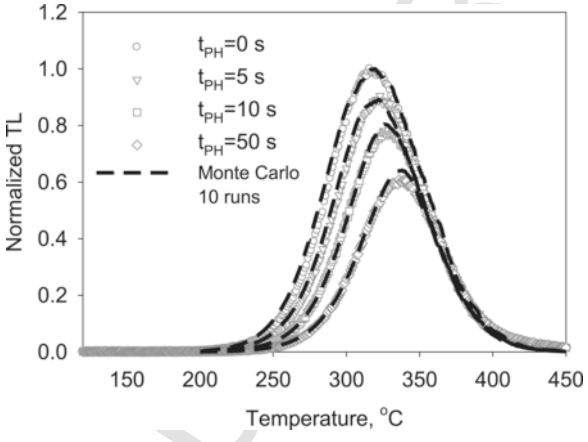

Fig. 4. The irradiated microcline KST4 sample was preheated to T_{PH}= 300 °C and this preheat temperature was held fixed for a variable preheat time t_{PH} = 0,5,10,50 s. It is assumed that these preheated samples can be described using a *truncated* distribution function, and the critical radius is treated as an adjustable fitting parameter. The MC results are shown as dashed lines, and the fitting parameters are: $E = 1.45$ eV, $A_{TL} = 3.5 \times 10^{12}$ s^{-1} ,and $r'_c = 0,\ 0.7,\ 0.77,\ 0.86$.

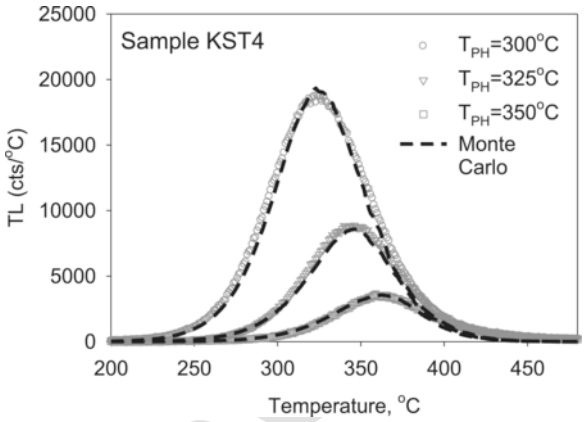

Fig. 5. The TL glow curves for a second set of measurements with a fixed preheat time $t_{PH} = 10$ s and a variable preheat *temperature* T_{PH}= 300, 325, 350 °C. The MC simulation are shown as dashed lines, and the critical distances are: $r'_c = 0.85,\ 1.13,\ 1.3$. The rest of the fitting parameters are the same as in Fig. 4.

critical radius r'_c up to infinity. This critical radius is treated as an adjustable modeling parameter in fitting the experimental data in Fig. 4, with the results of the MC simulation shown as dashed lines. The MC simulation were carried out with the parameters $E = 1.45$ eV, $A_{TL} = 3.5 \times 10^{12}$ s^{-1} and $\rho' = 0.015$. These numerical values are in close agreement with the more complex analysis presented recently by Polymeris et al. [25]. The values of the critical distance for the four MC simulations in Fig. 4 are: $r'_c = 0,\ 0.7,\ 0.77,\ 0.86$.

Fig. 5 shows the TL glow curves for a second set of measurements using the same sample, with a fixed preheat time $t_{PH} = 10$ s and a variable preheat *temperature* T_{PH}= {300, 325, 350} °C. The experimental data is compared with the results of the MC simulation shown as dashed lines. The values of the critical distance for the MC simulations in Fig. 5 are: $r'_c = 0.85,\ 1.13,\ 1.3$ and the rest of the fitting parameters E, A_{TL},ρ' are the same as in Fig. 4.

The overall results from Fig. 4 and 5 show that the TL glow curves for preheated samples can be described accurately using the truncated distributions characterized by the critical radius parameter r'_c. The MC method in this paper is then an attractive alternative method for analyzing this type of experimental data.

Fig. 6a shows a quantitative fitting of the experimental LM-IRSL data in Bulur and Göksu ([27], their Fig. 6b), in which they studied LM-IRSL signals in Na and K-feldspar samples. Similar data were previously analyzed by Kitis and Pagonis [3], by using approximate analytical expressions. Some of the experimental data of Bulur and Göksu [27] are shown in Fig. 6a together with the MC results (solid lines). The experimental data was normalized in order to show clearly the change of shape of the LM-IRSL curves as the stimulation temperature is increased. The fitting parameters are: $A_{LM-IRSL} = 0.63 - 0.90$ s^{-1},$\rho' = 0.018$. Once more, good agreement is seen between the MC simulation and the experiment. Fig. 6b shows an Arrhenius plot of the IR-stimulation probability *A(T)* obtained from the fittings of Fig. 6a. The straight line fit in Fig. 6b yields a thermal activation energy of $E = (0.029 \pm .001)$ eV. This value of E is of the same magnitude as previously reported values by Poolton et al. [30].

6. Discussion

The TL glow curves from feldspar samples have a rather unusual very broad shape, with full widths at half maximum (FWHM) of the order of ~80 K. It is generally accepted that these broad shapes are most likely due to either an underlying continuum of activation energies E, or alternatively to a continuum of frequency factors s. For a detailed examination of these two possibilities, the reader is referred to the extensive experimental study by Spencer [31].

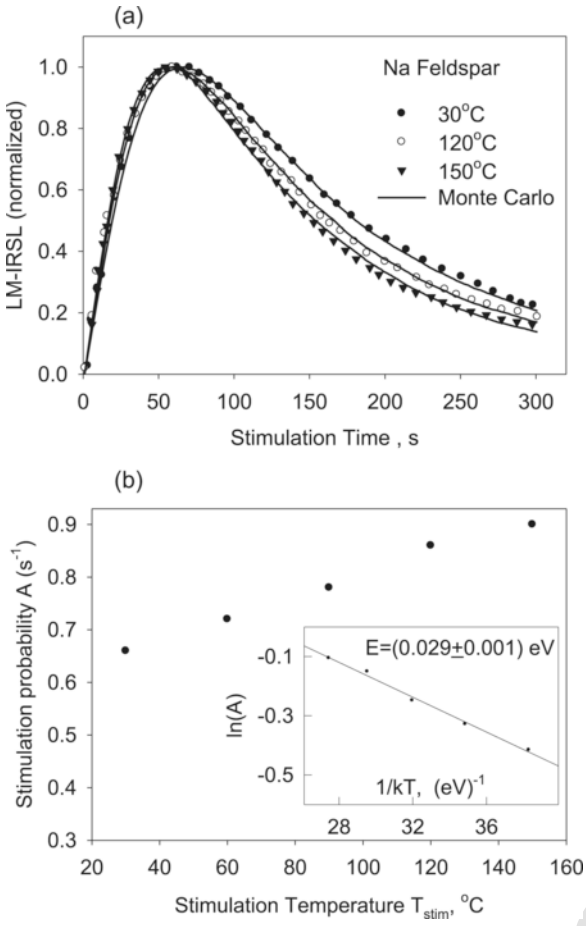

Fig. 6. (a) Quantitative fitting of the experimental LM-IRSL data in Bulur and Göksu [27], obtained by increasing the stimulation temperature in the Na-feldspar. (b) Arrhenius plot of the IR-stimulation probability $A(T)$ obtained from the MC simulations in (a). The inset shows the Arrhenius straight line fit, which yields a thermal activation energy of $E = (0.029 \pm .001)$ eV.

The equations developed in this paper offer a new *mathematical interpretation* of the broad shape of TL signals in feldspars, as follows. In the case of TL, $A_{TL} = s_{th}\exp[-E/k_BT]$ and Eq. (5) becomes:

$$\frac{\partial n(r',t)}{\partial t} = -\frac{s_{th}s_{tun}}{B\ \exp\left[-(\rho')^{-1/3}r'\right]} n(r',t) \exp\left[-E/k_BT\right]. \quad (16)$$

By defining an effective frequency factor s_{eff-TL}:

$$s_{eff-TL}(r') = \frac{s_{th}s_{tun}}{B\ \exp\left[-(\rho')^{-1/3}r'\right]}, \quad (17)$$

we obtain from Eq. (16):

$$\frac{\partial n(r',t)}{\partial t} = -s_{eff-TL}(r')\, n(r',t) \exp\left[-E/k_BT\right]. \quad (18)$$

For a constant distance r', Eq. (18) is identical to the well-known differential equation for TL glow curves following first order kinetics:

$$\frac{dn}{dt} = -sn\ \exp\left(-E/k_BT\right). \quad (19)$$

This analysis combined with the physical interpretation of Eqs. (10) and (13), suggests that the TL glow curve in feldspars can be considered as the summation of individual first order TL glow peaks with a distribution of effective frequency factors $s_{eff-TL}(r')$ which depend on the distances r' according to Eq. (17). For freshly irradiated feldspars the amplitudes of these individual TL glow curves also depend on the distances r', and are given by the peak-shaped function $3(r')^2\exp[-(r')^3]$. For samples which have undergone previous optical or thermal treatment, the distribution of amplitudes is given by a truncated distribution.

An example of this type of analysis is shown in the MC run of Fig. 7, where a TL glow curve is obtained mathematically as the sum of first order TL peaks.

Experimentally, it was demonstrated in multiple studies that the bulk TL signal of feldspar is composed of a continuous series of individual TL glow peaks (e.g. [25,32–34]). Related effects were observed also for charoite (Correcher et al., [35]) and lime-aluminosilicate glass (Discher, [36]). However, Pagonis et al. ([37]) used general order kinetics to describe the 'subpeak' resulting from the subtraction of two TL glow curves that were obtained following preheating to closely spaced temperatures. Similarly, general order kinetics were used to fit such 'subpeaks' in recent investigations exploring feldspar extracted from bedrock as a thermochronometer, yielding kinetic orders in the range ~1.5–2 for most samples (Brown and Rhodes, [38]; Brown et al. [39]; Biswas et al, [40]). One possible explanation for the discrepancy between modeling predictions and measured data could be that the temperature difference in the preheating experiments is not small enough to produce a single TL peak of first-order kinetics. In that case, the resulting subpeak would itself be composed of a small number of individual peaks that can be best described by general-order kinetics.

This mathematical description of luminescence signals in feldspars as the sum of first order signals also applies to CW-IRSL signals. In this case $A_{CW-IRSL}$ = constant and the corresponding effective frequency factor $s_{eff-CW-IRSL}(r')$ is now defined by:

$$s_{eff-CW-IRSL}(r') = \frac{A_{CW-IRSL}s_{tun}}{B\ \exp\left[-(\rho')^{-1/3}r'\right]}, \quad (20)$$

and Eq. (17) now becomes:

$$\frac{\partial n(r',t)}{\partial t} = -s_{eff-CW-IRSL}(r')\, n(r',t). \quad (21)$$

The solution of this equation for a constant value of r' is a single decaying exponential function of the time, which leads to the conclusion that the CW-IRSL signals from feldspars are the sum of exponential decay functions, with amplitudes given by the peak shaped function $3(r')^2\exp[-(r')^3]$.

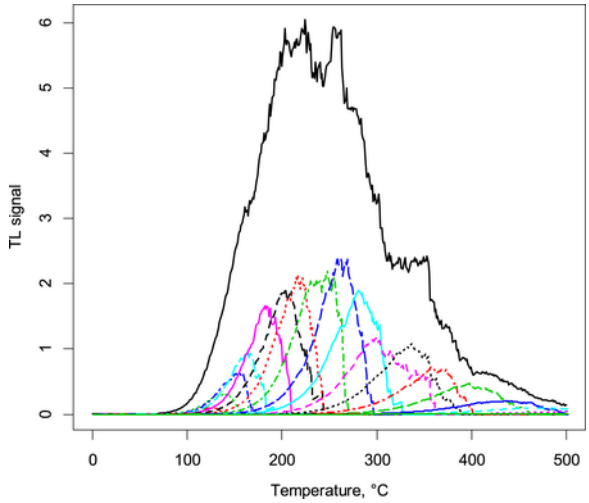

Fig. 7. Example of the output from the MC procedure for a TL glow curve, showing how the broad TL glow curves in feldspars can be considered as a sum of several first-order TL glow peaks with a distribution of amplitudes given by the symmetric function shown in Eq. (7).

7. Conclusions

The MC method presented in this paper is simple to implement, fast and accurate and reproduces the same results as the integrated numerical solution of the system of differential equations in Jain et al. [2]. An additional advantage is that the same method can also be used for truncated distributions of nearest neighbors, which describe luminescence signals from thermally or optically pretreated feldspar samples.

Another important conclusion from the previous section, is that the equations in this paper provide a new quantitative interpretation of the broad shape of TL glow curves in feldspars, as sums of first-order TL peaks. Similarly, the shape of CW-IRSL curves in feldspars can be described mathematically as the sums of first-order exponential decay functions. These are two new mathematical interpretations within the framework of the model by Jain et al. [2], which have not been pointed out previously in the literature.

The MC method presented here can also be extended to describe trap clustering effects in nanodosimetric materials. Future work will aim at combining these MC techniques in a comprehensive **R** [41] package.

Acknowledgements

The work by MD, AMK, VS and CS are supported by the project 'ULTIMO: Unifying Luminescence Models of quartz and feldspar' (DAAD PPP USA 2018, ID: 57387041).

The work of SK is financed by a program supported by the ANR – no ANR-10-LABX-52.

The authors also thank Dr. George Polymeris for providing a digital copy of the data shown in Fig. 2 and 3.

References

[1] V. Pagonis, R. Chen, C. Kulp, G. Kitis, Radiat. Meas. 106 (2017) 3–12.
[2] M. Jain, B. Guralnik, M.T. Andersen, J. Phys.: Condens. Matter 24 (2012) 385402, (12pp).
[3] G. Kitis, V. Pagonis, J. Lumin. 137 (2013) 109–115.
[4] G.S. Polymeris, V. Giannoulatou, I.K. Sfampa, N.C. Tsirliganis, G. Kitis, J. Lumin. 153 (2014) 245–251.
[5] I.K. Sfampa, G.S. Polymeris, N.C. Tsirliganis, V. Pagonis, G. Kitis, Nucl. Instrum. Method Phys. Res. B 320 (2014) 57–63.
[6] V. Pagonis, M. Jain, K.J. Thomsen, A.S. Murray, J. Lumin. 153 (2014) 96–103.
[7] G. Kitis, G.S. Polymeris, I.K. Sfampa, M. Prokic, N. Meriç, V. Pagonis, Radiat. Meas. 84 (2016) 15–25.
[8] G.S. Polymeris, I.K. Sfampa, M. Niora, E.C. Stefanaki, L. Malletzidou, V. Giannoulatou, V. Pagonis, G. Kitis, J. Lumin. 195 (2017) 216–224.
[9] M. Jain, R. Sohbati, B. Guralnik, A.S. Murray, M. Kook, T. Lapp, A.K. Prasad, K.J. Thomsen, J.P. Buylaert, Radiat. Meas. 81 (2015) 242–250.
[10] A. Mandowski, J. Swiatek, J. Philos. Mag. B65 (1992) 729–732.
[11] A. Mandowski, J. Swiatek, Radiat. Meas. 29 (1998) 415–419.
[12] A. Mandowski, Radiat. Meas. 43 (2008) 199–202.
[13] V. Pagonis, E. Gochnour, M. Hennessey, C. Knower Radiat. Meas. 67 (2014) 67–76.
[14] D.P. Landau, K. Binder, A Guide to Monte Carlo Simulations in Statistical Physics, 3rd ed., Cambridge University Press, 2013.
[15] V. Pagonis, P. Truong, Phys. B: Condens. Matter 531 (2018) 171–179.
[16] V. Pagonis, S. Bernier, F.M. Vieira, S. Steele, Nucl. Instrum. Methods Phys. Res. B 412 (2017) 198–206.
[17] V. Pagonis, C. Kulp, C.G. Chaney, M. Tachiya, J. Phys.: Condens. Matter 29 (2017) 365701.
[18] V. Pagonis, C. Kulp, J. Lumin. 181 (2017) 114–120.
[19] A. Mandowski, J. Phys. D: Appl. Phys. 38 (2005) 17–21.
[20] Y.S. Horowitz, I. Eliyahu, L. Oster, Radiat. Prot. Dosim. 172 (2015) 524–540.
[21] R. Chen, V. Pagonis, Thermally and Optically Stimulated Luminescence: a Simulation Approach, Wiley and Sons, Chichester, 2011.
[22] N. Salah, Radiat. Phys. Chem. 80 (2011) 1–10.
[23] H.T. Sun, Y. Sakka, Sci. Technol. Adv. Mater. 15 (2014) 014205, https://doi.org/10.1088/1468-6996/15/1/014205.
[24] G.S. Polymeris, E. Theodosoglou, G. Kitis, N.C. Tsirliganis, A. Koroneos, K.M. Paraskevopoulos, Mediterr. Archaelogy Archaeom. 13 (2013) 155–161.
[25] G.S. Polymeris, V. Pagonis, G. Kitis, Radiat. Meas. 97 (2017) 20–27.
[26] V. Pagonis, G. Polymeris, G. Kitis, Radiat. Meas. 82 (2015) 93–101.
[27] E. Bulur, H.Y. Göksu, Radiat. Meas. 30 (1999) 505–512.
[28] V. Pagonis, H. Phan, D. Ruth, G. Kitis, Radiat. Meas. 58 (2013) 66–74.
[29] S.W.S. McKeever, Thermoluminescence of Solids, Cambridge University press, 198548.
[30] N.R.J. Poolton, R.H. Kars, J. Wallinga, A.A.J. Bos, J. Phys. Cond. Matter 21 (2009) 485505.
[31] Joel Spencer The Development of Luminescence Methods to Measure Thermal Exposure in Lithic and Ceramic Materials (Ph.D. thesis) 1996 (available online at) http://theses.gla.ac.uk/3557/
[32] T. Sakurai, R.K. Gartia, J. Appl. Phys. 82 (1997) 5722–5727.
[33] J. Garcia-Guinea, V. Correcher, A. Delgado, L. Sanchez-Munoz, Radiat. Meas. 37 (2003) 473–477.
[34] V. Correcher, J.M. Gomez-Ros, J. Garcia-Guinea, Radiat. Meas. 38 (2004) 689–693.
[35] V. Correcher, J.M. Gomez-Ros, J. Garcia-Guinea, M. Lis, L. Sanchez-Munoz, Radiat. Meas. 43 (2008) 269–272.
[36] M. Discher . Lumineszenzuntersuchungen an Körpernah Getragenen Gegenständen für die Notfalldosimetrie (Diploma thesis) Technical University Munich Munich 2015
[37] V. Pagonis, P. Morthekai, G. Kitis, Geochronometria 41 (2014) 168–177.
[38] N.D. Brown, E.J. Rhodes, Radiat. Meas. 96 (2017) 53–61.
[39] N.D. Brown, E.J. Rhodes, T.M. Harrison, Quat. Geochronol. 42 (2017) 31–41.
[40] R.H. Biswas, F. Herman, G.E. King, J. Braun, Earth Planet. Sci. Lett. 495 (2018) 56–68.
[41] R. Core Team, R: A Language and Environment for Statistical Computing 2018 ⟨https://r-project.org⟩.